Comprehensive Monte Carlo study of patient doses from cone-beam CT imaging in radiotherapy

T E Marchant[1,2] and K D Joshi[2]

[1]The University of Manchester, Manchester Academic Health Science Centre, The Christie NHS Foundation Trust, Manchester, M20 4BX, UK.
[2]Christie Medical Physics and Engineering, The Christie NHS Foundation Trust, Manchester, M20 4BX, UK.

E-mail: tom.marchant@christie.nhs.uk

Abstract. Accurate knowledge of ionizing radiation dose from cone-beam CT (CBCT) imaging in radiotherapy is important to allow concomitant risks to be estimated and for justification of imaging exposures. This study uses a Monte Carlo CBCT model to calculate imaging dose for a wide range of imaging protocols for male and female patients. The Elekta XVI CBCT system was modeled using GATE and simulated doses were validated against measurements in a water tank and thorax phantom. Imaging dose was simulated in the male and female ICRP voxel phantoms for a variety of anatomical sites and imager settings (different collimators, filters, full and partial rotation). The resulting dose distributions were used to calculate effective doses for each scan protocol. The Monte Carlo simulated doses agree with validation measurements within 5 % and 10 % for water tank and thorax phantom respectively. Effective dose for head CBCT scans was generally lower for scans centred on the pituitary than the larynx (0.03 mSv vs. 0.06 mSv for male ICRP phantom). Pelvis CBCT scan effective dose was higher for the female than male phantom (5.11 mSv vs. 2.80 mSv for M15 collimator scan), principally due to the higher dose received by gonads for the female scan. Medium field of view thorax scan effective doses ranged from 1.38 - 3.19 mSv depending on scan length and phantom sex. Effective dose for half rotation thorax scans with offset isocentre varied by almost a factor of three depending on laterality of the isocentre, patient sex and imaged field length. The CBCT imaging doses simulated here reveal large variations in dose depending on imaging isocentre location, patient sex and partial rotation angles. This information may be used to estimate risks from CBCT and to optimize CBCT imaging protocols.

Keywords: Cone-beam CT, Image-guided radiotherapy, Monte Carlo simulation, Imaging dose.
PACS numbers: 87.53.Bn (Dosimetry/exposure assessment), 87.55.K- (MC methods), 87.57.Q- (CT)

1. Introduction

Cone beam CT (CBCT) imaging is commonly used in radiotherapy for verification of patient and target position [1,2]. Use of CBCT imaging can improve the quality of radiotherapy by reducing geometric errors, leading to the use of smaller margins, and providing potential for adaptive radiotherapy. However use of CBCT is not without risk to the patient due to

the additional dose of ionizing radiation involved. Accurate knowledge of patient dose from CBCT is therefore important so that concomitant risks can be estimated allowing justification of additional imaging. This is particularly important because CBCT imaging is typically repeated, sometimes at every fraction of treatment, leading to potentially large total doses.

Imaging doses from CBCT in radiotherapy have been reported in many studies since its introduction in the early 2000s [3]. Reported doses are either based on direct measurements, or on modeling often using Monte Carlo (MC) methods. Dose measurements are most commonly made in phantoms, which may represent patient anatomy to a greater or lesser extent [4–9]. Measurements are time consuming to perform due to the large number of measurement points required to represent the full distribution of dose in the patient. Effective dose estimates, which allow the linking of dose to risk, require the mean absorbed dose to each organ (subsequently referred to as "organ dose") to be measured as defined in ICRP103 [10]. Some studies [6,7,11–13] have calculated effective doses for CBCT based on dose measurements at the various organ locations, however this involves uncertainty due to the non-uniformity of dose within each organ [14].

Monte Carlo methods have been used to overcome the limitations of phantom measurements [14–19]. MC offers the flexibility to simulate full 3D dose distributions within a range of objects including voxel phantoms based on actual patient anatomy. However, it can be time consuming to achieve acceptable statistical errors with MC simulations, and the models must be validated to ensure they accurately reproduce doses within complex patient anatomy.

Most studies of CBCT dose have reported doses for a relatively small number of standard imaging protocols – e.g. head, thorax and pelvis. In clinical practice CBCT imaging is applied at wide range of anatomical sites and there are many imaging protocol variations, for example different fields of view (FOVs), filters, full and half rotation scans. The effect of these variations on CBCT imaging dose has not been comprehensively studied. Also CBCT doses in the literature are usually reported only for male patients. Some quote doses based on female patient image sets or phantoms [11,13,17,20–23], but few compare male and female doses from the same imaging protocol [24].

In this study we have developed an MC model of the Elekta XVI CBCT imaging system (Elekta AB, Stockholm, Sweden). We use this model to calculate organ and effective doses in the ICRP male and female voxel phantoms [25] for a wide range of imaging sites (including male and female, brain, larynx, lung (left, right and central), prostate, cervix, breast (left and right)) and scanning protocols (including small, medium and large FOV, with and without bow-tie filter, full and half rotation scans with various angular ranges). The ICRP computational phantoms were previously used in dosimetry studies of Varian Truebeam linac-integrated CBCT [26] and of dental CBCT [27].

2. Methods and materials

2.1. Monte Carlo model of Elekta XVI CBCT

The Elekta XVI CBCT system was modeled using the Geant4 Application for Tomographic Emission (GATE) [28]. GATE has previously been used to model a wide range of medical physics applications including proton therapy, Megavoltage X-ray therapy and kilovoltage X-ray CBCT [18,29]. The results shown in this report were calculated using GATE v7.1 (March 2015), which is based on Geant4 v10.1. The Geant4 "physics list" mechanism [30] is used to specify processes to be included in the simulation. All simulations were done using the EMLivermore physics list, which is optimized for accuracy of electron and photon physics in the low (kilovoltage) energy range. This physics list has been used and recommended in other studies of kV X-ray imaging/therapy [31,32]. The GATE XVI model includes the following components:

2.1.1. X-ray source A "virtual" X-ray source has been defined using the general particle source object in GATE. This allows an X-ray source of arbitrary shape with user-defined energy spectrum to be created. Energy spectra corresponding to peak tube voltages of 100 kV and 120 kV with filtration equivalent to 5.25 mm Al were generated according to the methods described in Boone 1997 [33]. The source has been defined as a rectangle of size 0.8 mm x 0.4 mm, to match the size of the focal spot given in the XVI system documentation. The rectangular source is embedded a small distance (2.5 μm) below the surface of a tungsten disc, representing the generation of X-rays close to the surface of the anode in the X-ray tube. The depth of the source within the anode reproduces the differential self-absorption of X-rays within the anode as a function of emission angle (anode-heel effect), with the depth used adjusted empirically to best match dose profiles across the beam measured in water (see section 2.2.1). Simulations of 120 keV electrons incident on a tungsten target showed that 2.5 μm is close to the mean depth of interaction. The tungsten target with embedded photon source is rotated at an angle of 17.5° from the beam axis to simulate the anode angle of the X-ray tube (14°) plus the tilt of the X-ray tube mounting relative to the central beam axis. The centre of the photon source is located at 100 cm from the centre of rotation of the CBCT system (nominal linac isocentre).

2.1.2. Collimators The XVI system has a series of interchangeable collimator cassettes each containing a lead sheet with cut-outs of different size and shape to define the different X-ray field sizes available. Collimators are identified by a letter (S, M or L) indicating the reconstructed FOV diameter, and a number (10, 15, 20) indicating the FOV length. Nominal FOV sizes for the different collimators are given in Spezi 2009 [34]. Each collimator is modeled as a 3.2 mm thick sheet of lead with appropriate cutouts. Small adjustments ($<$1 mm) were made to the nominal cut-out dimensions and offsets to best match measured profiles. Collimators are positioned at a distance of 20 cm from the X-ray source along the beam axis towards the centre of rotation. The collimator cassettes also have thin plastic covers on either

side which are included in the model as 1 mm thicknesses of PET-G.

2.1.3. Bow tie filter The XVI CBCT system contains a removable aluminium (Al2017 alloy) bow tie filter (referred to as F1). The F1 filter was modeled according to the specifications in the XVI documentation, with the curved shape of the filter approximated in GATE as a series of 100 trapezoids. The centre of the bow tie filter is located at a distance of 25 cm from the X-ray source. The bow tie filter may be removed and replaced with an empty filter cassette, referred to as F0.

2.1.4. Gantry rotation Rotation of the CBCT gantry has been modeled in GATE through rotation of the patient volume (containing the representation of the patient or phantom being exposed). Rotations are applied about an axis running along the length of the treatment couch and passing through the linac isocentre. This allows the patient volume to be exposed from any gantry angle. In practice the rotation speed of the XVI system is not constant throughout the CBCT acquisition. Initial projection images are acquired with the gantry static in the start position, which then accelerates to a constant speed for most of the rotation, but then decelerates to a stop over the final few degrees of the rotation. Full rotation acquisitions were modeled in GATE as projections from 200 different gantry angles sampled at equal time increments from a measured gantry angle trajectory. A similar rotation trajectory was measured for half rotation scans and used to model these acquisitions, also as 200 discrete projection angles. Figure 1 illustrates rotation of the gantry for the head and neck (H&N) half scan protocol starting at -40° and finishing at +160°. Specified gantry angles always refer to the position of the megavoltage (MV) linac head with 0° being directly above the patient couch. The gantry can rotate in either direction to ±180°, but cannot rotate past 180°. The kV tube is mounted on the gantry with an offset of +90° from the linac head as shown in figure 1.

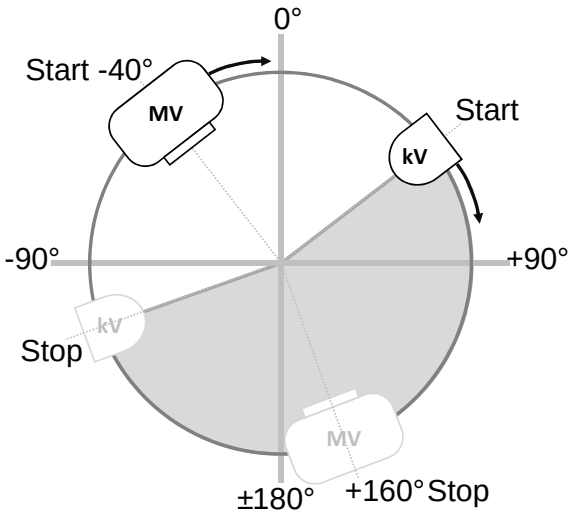

Figure 1. Rotation of the XVI gantry (view in direction of gantry). Marked gantry angles indicate the position of the MV linac head. Start and stop positions for H&N scan half rotation are shown with the shaded segment indicating angles traversed by the kV beam.

2.1.5. Dose output from GATE Dose output in GATE is facilitated using "Dose Actors" which can be defined as a 2D or 3D arrays covering a region in space or to coincide with the voxel locations of an image based phantom. The absorbed dose to the material in each voxel is returned by the dose actor. Simulation times in GATE were reduced by using the split exponential track length estimator dose actor (seTLE, introduced in GATE7.1), which makes use of trajectory splitting and exponential track-length estimator methods [35] to improve the efficiency of simulations.

2.2. Model validation

The GATE XVI model has been validated using dose measurements in a water tank and in an anthropomorphic thorax phantom.

2.2.1. Water tank profiles Three-dimensional dose distributions have been measured in a water-filled plotting tank (PTW MP3 tank) using a small volume ionization chamber (PTW Semiflex 31002). The gantry was rotated to -90° to position the kV source directly above the water tank with the beam aiming downwards into the water, and with kV source to surface distance of 75 cm. X, Y and depth profiles were acquired for each collimator with the F0 and F1 filters and at 100 and 120 kV. Profiles were scanned with a spatial resolution of 2 mm between measurement points in the beam penumbra and build-up regions and 5 mm between points elsewhere. A measurement time of 2 s per point was used. The X-ray tube was set to deliver 1.6 mAs per frame and 5 frames per second. The plotting tank was modeled in GATE as a cube of water and dose profiles corresponding to those measured were simulated with a spatial resolution of 2 mm. The GATE profiles were normalized and compared to the measurements.

2.2.2. Model calibration Dose measurements were made in head and thorax anthropomorphic phantoms in order to calibrate the MC simulated doses, using a procedure similar to that of Ding et al. [15]. These measurements were used to derive a Monte Carlo calibration factor f_{MC} :

$$D = f_{MC} D_{MC}$$

which converts simulated dose per photon, D_{MC}, into dose delivered by the CBCT system per mAs, D. The dose per mAs can then be scaled by the total mAs for the CBCT protocol to give the dose for that scan. Separate MC calibration factors are required for each simulated source energy (kVp).

Calibration measurements for the 100 kV beam were made using thermoluminescent dosimeters (TLDs) (Harshaw TLD-100H 3 x 3 x 1 mm chips) at various locations in a head phantom (CIRS ATOM 702), using a clinical head and neck scan exposure (S20 collimator). TLD measurement locations in the head phantom are shown in figure 3a, with two TLD chips being placed at each location. Measurements for the 120 kV beam were made in a thorax phantom (CIRS 002LFC) using a small volume ionization chamber (PTW semiflex 31002).

Thorax phantom measurements included both static beam angle and rotational exposures using the M20 chest preset. Measurement locations in the thorax phantom are shown in figure 3c. Similar to previous studes [15,36], anthropomorphic phantoms were used for the calibration measurements because they allow clinical scan protocols to be used, including rotational acquisition and realistic patient geometry. Both TLDs and the small volume ionization chamber were first calibrated in the XVI beam by inter-comparison in air with a Radcal 10x6-6cc chamber (itself calibrated traceable to national standards).

Dose measurements at each location in the phantom were compared to GATE simulations of the same exposures, using voxelized representations of the same phantoms (CT scans). The MC calibration factor at each kV was determined by minimizing the mean difference between measurements and simulations. Variations of the dose differences at each location in the phantom were also used to validate the simulated dose distribution within an anthropomorphic phantom containing materials of different tissue types (lung, soft-tissue, bone) from rotational exposures.

2.3. Simulation of patient CBCT doses

Dose from a full range of CBCT imaging protocols was simulated using the ICRP male and female computational phantoms. The ICRP phantoms are based on medical image data of real people yet are consistent with reference anatomical parameters given in ICRP report 89 [37]. The voxel phantoms consist of an organ type and material composition specified at each voxel. The voxel phantom was imported into the GATE simulation with the appropriate material specified at each voxel. For each CBCT protocol simulated 10^7 primary X-rays were generated, and doses were recorded using the seTLE dose actor with primary and secondary multiplicities of 200 and 400 respectively. The full phantom body length was included in each simulation and the dose scoring array was defined to cover the whole phantom with a voxel resolution matching the ICRP phantom definition (2.1 x 2.1 x 8.0 mm for the male phantom, 1.8 x 1.8 x 4.8 mm for the female phantom). Mean organ doses were calculated by averaging the dose in all voxels belonging to each organ. Organs with multiple parts (e.g. left and right breast) were considered to be part of a combined organ for the purposes of calculating the mean dose.

Doses were simulated from all default imaging protocols in XVI version 5.0. H&N protocols were simulated with both pituitary and larynx positioned at the isocentre, to represent the range of different locations at which the H&N protocol may be applied. Pelvis protocols were centred on prostate for the male phantom and on uterus for the female phantom. Additional protocols for lung and breast imaging that are used in our institution were also simulated. Half rotation lung protocols (Small FOV) are used in cases where the isocentre is laterally offset from the patient midline, preventing full rotation of the gantry around the patient. Different gantry start and stop angles are required depending on the laterality of the isocentre, and the isocentre location used was the centre of either the left or right lung. Large FOV lung protocols were also simulated, as well as half rotation protocols for left and right breast imaging. In total 41 CBCT image acquisitions were simulated.

3. Results

3.1. Model validation and calibration

Dose distributions in the water tank showed good agreement between simulations and measurements, with differences less than 5% in all areas excluding beam penumbras. Figure 2 shows sample profiles for S20, M20 and L20 collimators. Profiles for other collimators both with and without the bow tie filter showed similar levels of agreement.

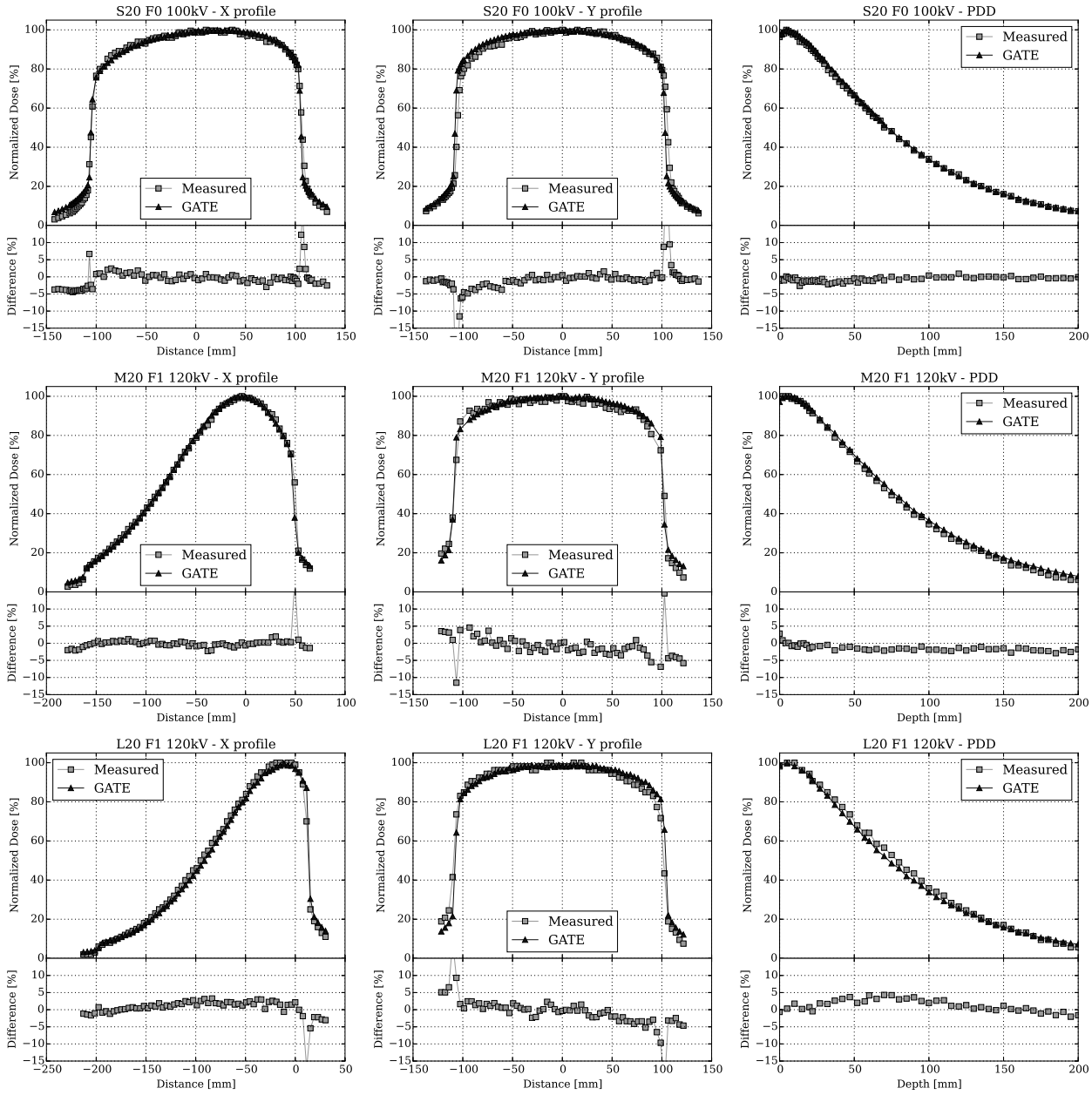

Figure 2. Comparison of simulated and measured dose profiles in a water tank.

MC calibration factors, f_{MC}, derived from the head and thorax phantom measure-

ments/simulations were 2.61 x 10^{11} photons per mAs at 100 kV, and 5.63 x 10^{11} photons per mAs at 120 kV. Dose distributions in the head phantom at 100 kV and in the thorax phantom at 120 kV showed good agreement with GATE simulations, shown in figure 3b and figure 3d. The difference between measured and simulated dose was less than 10% at all points (range -8% to +7% for head phantom, -9% to +7% for thorax phantom) with standard deviation of 5.4% for head phantom and 4.6% for the thorax phantom.

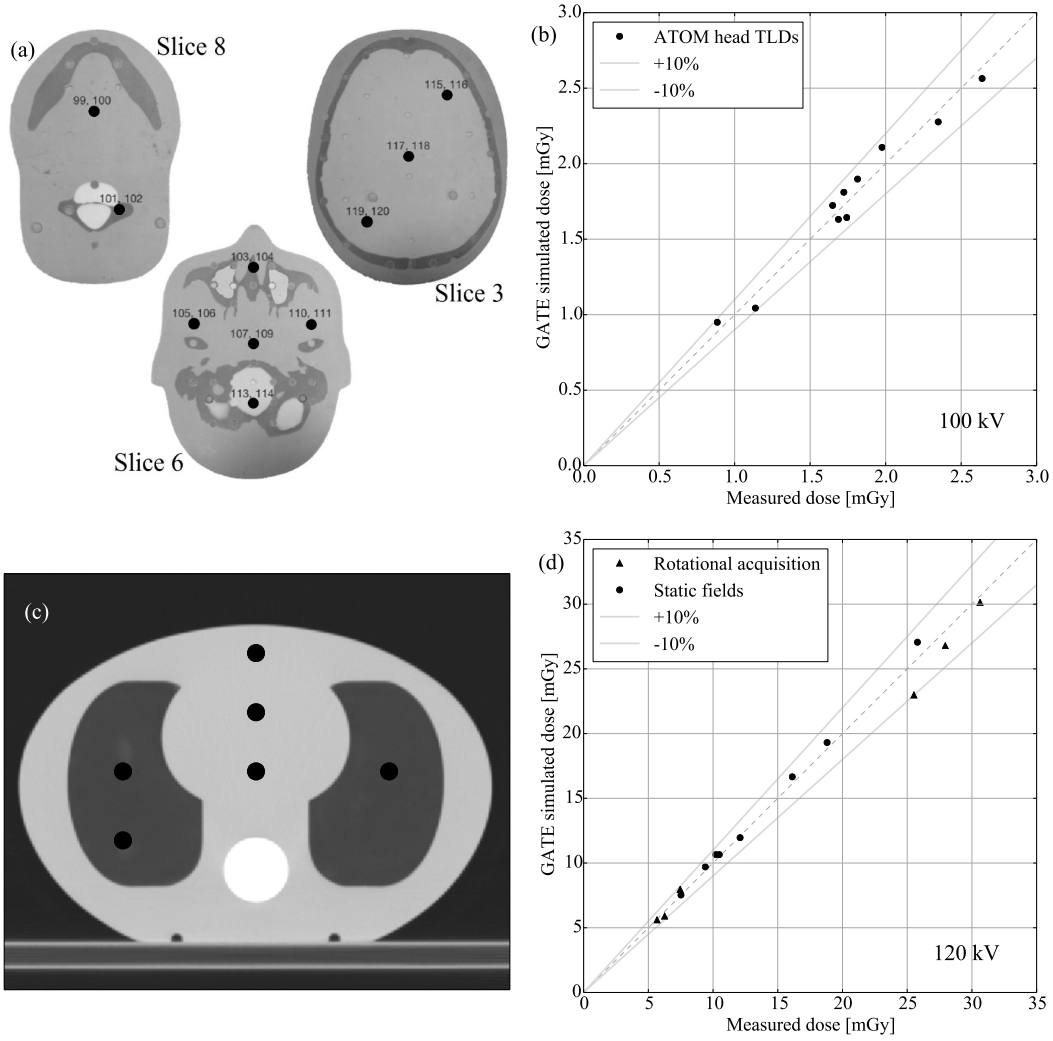

Figure 3. (a) Dose measurement locations in the ATOM head phantom (black circles). (b) Comparison of measured and simulated doses in the ATOM head phantom. (c) Dose measurement locations in the CIRS thorax phantom (black circles). (d) Comparison of measured and simulated doses in the CIRS thorax phantom.

3.2. Simulation of patient CBCT doses

Each simulation of CBCT scan dose in the ICRP phantom using 10^7 primary photons took approximately 2 hours to simulate using an AMD Opteron system with 64 2.3 GHz cores. Repeat simulations showed statistical uncertainty in effective dose estimates below 1 %.

Table 1 shows the organ and effective doses simulated in the ICRP phantom for head and neck CBCT scans. Effective doses are higher for scans with the S20 collimator than the S10 collimator due to the longer field length, although this is mitigated by the lower total mAs used for the "Fast" S20 head and neck protocols. Effective doses are also higher for scans centred on the larynx than those centred on the pituitary mainly due to the higher doses received by thyroid, oesophagus and lung. Eye lens doses, also shown in table 1, are higher for scans centred on pituitary because the eyes are within the imaged field. However the partial rotation from gantry angle -40° to +160° results in higher doses at the posterior of the head, thus minimizing dose to the eye lens. Figure 4 shows example dose distributions for head and neck CBCT scans in the male ICRP phantom, illustrating the different scan FOVs simulated and the asymmetry of dose due to partial rotation scanning.

Table 1: Organ and effective doses simulated in the ICRP phantoms for head and neck (H&N) CBCT scans. [a]Half rotation -40° to +160°.

Preset	*H&N S10*	*H&N S10*	*H&N S10*	*H&N S10*	*Fast H&N S20*	*Fast H&N S20*	*Fast H&N S20*	*Fast H&N S20*
Isocentre	Pituitary	Pituitary	Larynx	Larynx	Pituitary	Pituitary	Larynx	Larynx
Sex M/F	F	M	F	M	F	M	F	M
kV	100	100	100	100	100	100	100	100
Collimator	S10	S10	S10	S10	S20	S20	S20	S20
Filter	F0	F0	F0	F0	F0	F0	F0	F0
Total mAs	36.6	36.6	36.6	36.6	18.3	18.3	18.3	18.3
Rotation	half [a]	half [a]	half [a]	half [a]	half [a]	half [a]	half [a]	half [a]
Organ Doses [mGy]								
Bone marrow (red)	0.13	0.08	0.11	0.07	0.11	0.06	0.12	0.07
Colon	0.00	0.00	0.00	0.00	0.00	0.00	0.00	0.00
Lung	0.01	0.00	0.08	0.06	0.01	0.01	0.16	0.12
Stomach	0.00	0.00	0.00	0.01	0.00	0.00	0.01	0.01
Breast	0.00	0.00	0.02	0.01	0.01	0.00	0.07	0.01
Gonads	0.00	0.00	0.00	0.00	0.00	0.00	0.00	0.00
Bladder	0.00	0.00	0.00	0.00	0.00	0.00	0.00	0.00
Oesophagus	0.02	0.01	0.21	0.19	0.07	0.04	0.18	0.14
Liver	0.00	0.00	0.01	0.01	0.00	0.00	0.01	0.01
Thyroid	0.04	0.01	0.55	0.56	0.20	0.05	0.32	0.31
Bone surface	0.44	0.42	0.33	0.26	0.33	0.29	0.38	0.30
Brain	0.63	0.62	0.03	0.01	0.39	0.37	0.13	0.06
Salivary glands	0.66	0.56	0.47	0.26	0.48	0.46	0.48	0.45
Skin	0.05	0.05	0.06	0.05	0.05	0.04	0.07	0.06
Remainder	0.07	0.06	0.10	0.05	0.06	0.05	0.09	0.07
Eye lens	0.59	0.56	0.03	0.01	0.30	0.28	0.29	0.04
Effective Dose [mSv]	**0.05**	**0.03**	**0.08**	**0.06**	**0.05**	**0.03**	**0.09**	**0.06**

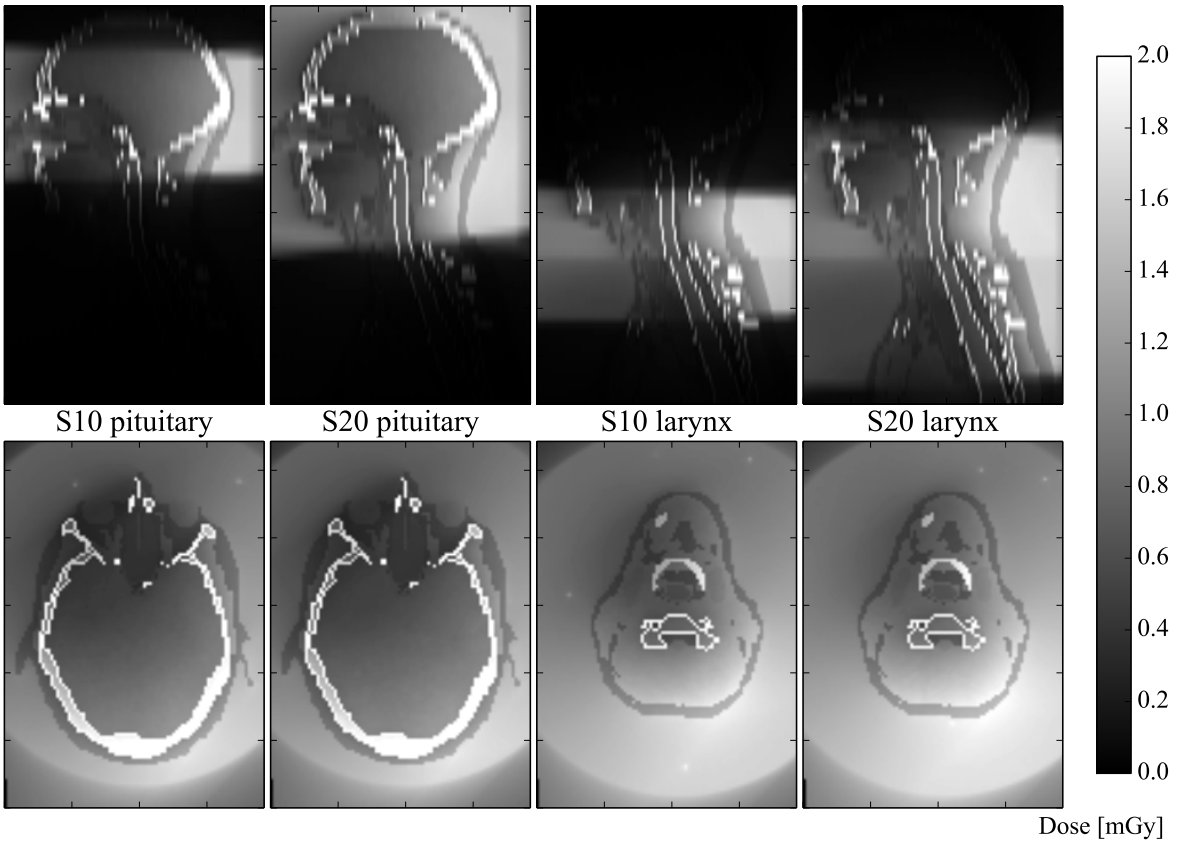

Figure 4. Simulated dose distributions in the ICRP male phantom for CBCT scans of head and neck region.

Table 2 shows the organ and effective doses simulated in the ICRP phantom for pelvis CBCT scans. Effective doses increase with exposed field length and with scan total mAs. The exposed organs within the FOV also have a significant influence on effective dose. For example "Pelvis M15" dose is 1.8 times higher for the female than the male phantom. This is principally due to the much higher dose to gonads and colon. A greater proportion of these organs is within the exposed field for the female phantom than for the male phantom, due to their different anatomical positions and the different scan centre locations (uterus and prostate). Figure 5 and figure 6 show example dose distributions for pelvis CBCT scans in the male and female ICRP phantoms, illustrating the different scan FOVs simulated. The asymmetry of doses between right and left is caused by the gantry starting and stopping with the kV tube on the patient right side.

Table 2: Organ and effective doses simulated in the ICRP phantoms for pelvis CBCT scans. [b]Half rotation: Gantry angle -130° to +70°.

Preset	*Prostate M10*	*Prostate M15*	*Pelvis M15*	*Pelvis M15*	*Pelvis M20*	*Pelvis M20*	*Pelvis L20*	*Pelvis L20*	*Fast Prostate Seed S10*
Isocentre	Prostate	Prostate	Uterus	Prostate	Uterus	Prostate	Uterus	Prostate	Prostate
Sex M/F	M	M	F	M	F	M	F	M	M
kV	120	120	120	120	120	120	120	120	120
Collimator	M10	M15	M15	M15	M20	M20	L20	L20	S10
Filter	F1	F1	F1	F1	F1	F1	F1	F1	F0
Total mAs	1689.6	1689.6	1056.0	1056.0	1056.0	1056.0	1689.6	1689.6	46.8
Rotation	full	full	full	full	full	full	full	full	half [b]
Organ Doses [mGy]									
Bone marrow (red)	5.30	6.52	4.76	4.08	6.73	5.82	7.88	6.98	0.29
Colon	2.23	3.72	8.84	2.33	15.45	4.26	17.03	4.53	0.09
Lung	0.09	0.11	0.10	0.07	0.17	0.11	0.23	0.15	0.00
Stomach	0.15	0.20	0.24	0.13	0.53	0.22	0.68	0.28	0.00
Breast	0.11	0.13	0.09	0.08	0.15	0.13	0.20	0.19	0.00
Gonads	6.46	13.91	22.11	8.70	24.52	31.22	27.49	34.34	0.36
Bladder	28.02	35.12	27.98	21.95	29.98	25.48	34.63	29.83	1.39
Oesophagus	0.06	0.08	0.07	0.05	0.13	0.08	0.17	0.13	0.00
Liver	0.14	0.19	0.21	0.12	0.45	0.24	0.56	0.31	0.00
Thyroid	0.07	0.08	0.10	0.05	0.13	0.08	0.16	0.12	0.00
Bone surface	11.52	14.69	9.91	9.18	15.01	14.07	18.02	16.95	0.60
Brain	0.04	0.05	0.04	0.03	0.06	0.05	0.08	0.07	0.00
Salivary glands	0.08	0.09	0.06	0.06	0.10	0.08	0.12	0.13	0.00
Skin	3.43	4.61	3.26	2.88	5.12	4.70	6.41	5.86	0.19
Remainder	3.30	3.94	3.22	2.46	4.27	3.24	5.06	4.00	0.15
Effective Dose [mSv]	**3.14**	**4.48**	**5.11**	**2.80**	**6.67**	**5.37**	**7.60**	**6.13**	**0.16**

Table 3, table 4, and table 5 show simulated organ and effective doses for CBCT scans of the thorax. Female organ doses are generally slightly higher due to smaller dimensions of the phantom. Doses increase with field length due to greater scatter and greater number of body organs within the exposed region. The "Symmetry 4D" preset has the highest dose due to the higher mAs and use of F0 rather than F1 filter. SFOV half rotation effective doses vary by almost a factor of three depending on the laterality of the isocentre, patient sex and imaged field length. Dose to breast from half rotation breast CBCT scans is also highly variable depending on the partial rotation used, ranging from 1.1 mGy to 5.5 mGy. The degree of dose sparing that can be achieved to the contralateral breast is limited by the partial rotation that can be used, which cannot extend past 180°. This results in the better contralateral breast sparing achieved for left than right breast scans. Figure 7 and figure 8 show simulated dose distributions from CBCT scans of the chest with MFOV and SFOV respectively.

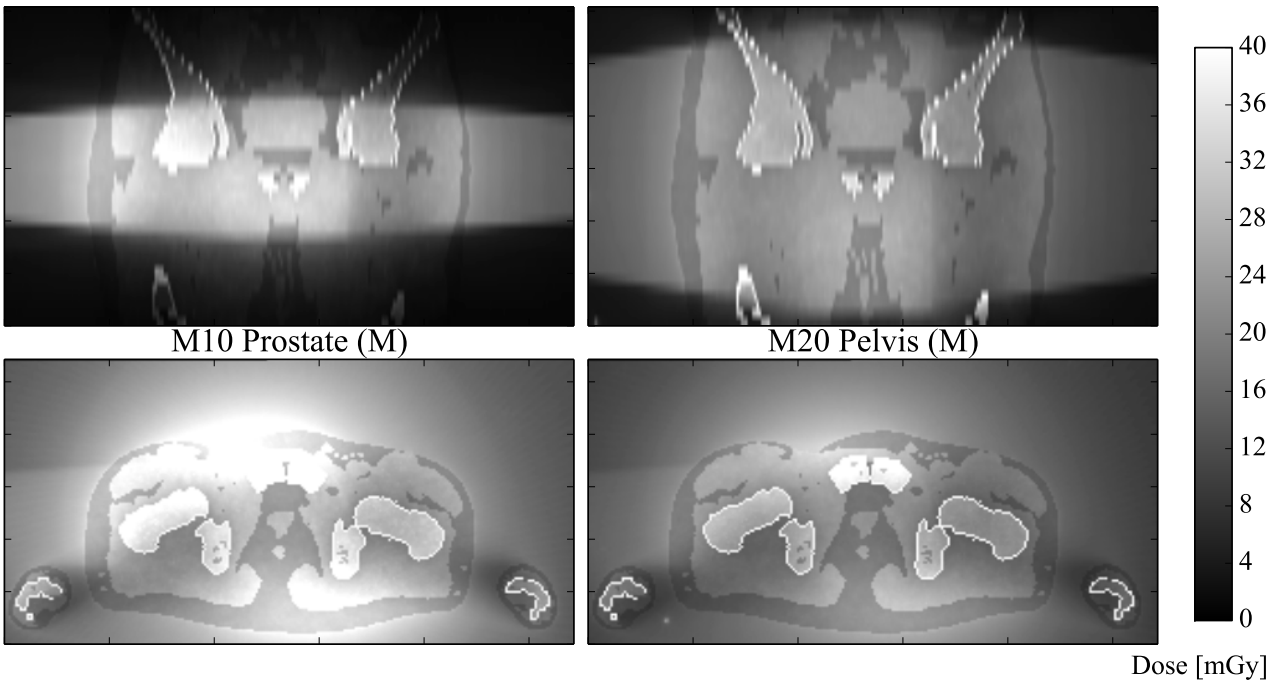

Figure 5. Simulated dose distributions in the ICRP male phantom for pelvis CBCT scans.

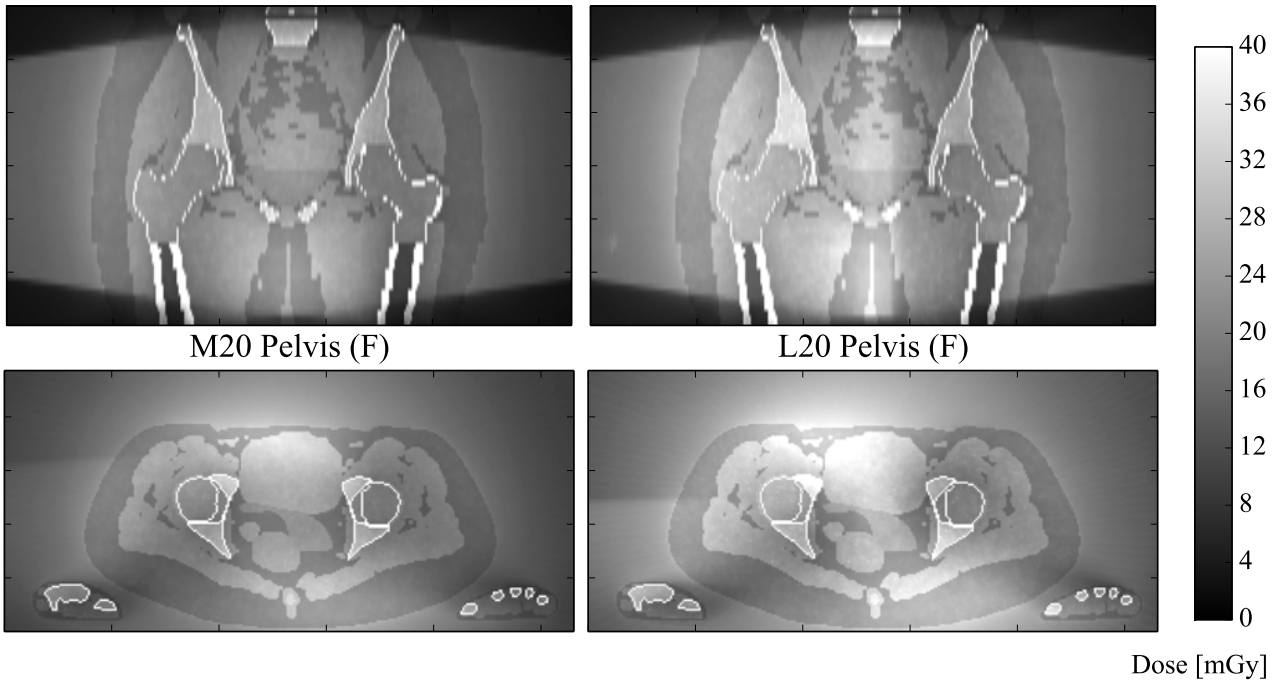

Figure 6. Simulated dose distributions in the ICRP female phantom for pelvis CBCT scans.

Table 3: Organ and effective doses simulated in the ICRP phantoms for MFOV and 4D chest CBCT scans. [c]Half rotation: Gantry angle -180° to +20°.

Preset	*Chest M10*	*Chest M10*	*Chest M15*	*Chest M15*	*Chest M20*	*Chest M20*	*Symmetry 4D*	*Symmetry 4D*
Isocentre	Lung centre	Lung centre	Lung centre	Lung centre	Lung centre	Lung centre	Lung centre	Lung centre
Sex M/F	F	M	F	M	F	M	F	M
kV	120	120	120	120	120	120	120	120
Collimator	M10	M10	M15	M15	M20	M20	S20	S20
Filter	F1	F1	F1	F1	F1	F1	F0	F0
Total mAs	264.0	264.0	264.0	264.0	264.0	264.0	312.0	312.0
Rotation	full	full	full	full	full	full	half [c]	half [c]
Organ Doses [mGy]								
Bone marrow (red)	0.76	0.63	1.04	0.88	1.69	1.45	3.53	3.20
Colon	0.04	0.12	0.06	0.18	0.12	0.48	0.21	1.30
Lung	4.85	3.81	5.82	4.56	6.76	5.36	14.04	13.22
Stomach	0.67	0.75	1.16	1.37	3.26	3.27	8.66	9.98
Breast	4.76	3.72	5.15	4.13	5.45	4.41	22.18	19.77
Gonads	0.01	0.01	0.02	0.02	0.03	0.03	0.03	0.03
Bladder	0.01	0.01	0.02	0.02	0.03	0.03	0.04	0.03
Oesophagus	2.92	2.32	3.95	3.10	5.92	4.61	10.75	8.87
Liver	0.90	0.88	1.72	1.53	4.37	3.61	10.46	9.13
Thyroid	0.83	0.69	1.39	1.10	8.80	7.68	21.58	19.19
Bone surface	2.42	2.27	3.23	3.02	4.93	4.61	8.70	8.19
Brain	0.04	0.03	0.06	0.04	0.12	0.09	0.18	0.12
Salivary glands	0.18	0.12	0.26	0.17	0.57	0.37	1.26	0.79
Skin	0.65	0.51	0.84	0.67	1.26	1.03	3.12	2.48
Remainder	1.05	0.87	1.46	1.24	2.37	2.12	5.18	4.79
Effective Dose [mSv]	**1.67**	**1.38**	**2.09**	**1.75**	**3.19**	**2.75**	**8.30**	**7.88**

Table 4: Organ and effective doses simulated in the ICRP phantoms for SFOV chest CBCT scans. [c]Half rotation: Gantry angle -180° to +20°. [d]Half rotation: Gantry angle -80° to +120°.

Preset	*Left Lung S10*	*Left Lung S10*	*Left Lung S20*	*Left Lung S20*	*Right Lung S10*	*Right Lung S10*	*Right Lung S20*	*Right Lung S20*
Isocentre	L lung	L lung	L lung	L lung	R lung	R lung	R lung	R lung
Sex M/F	F	M	F	M	F	M	F	M
kV	120	120	120	120	120	120	120	120
Collimator	S10	S10	S20	S20	S10	S10	S20	S20
Filter	F1	F1	F1	F1	F1	F1	F1	F1
Total mAs	117.1	117.1	117.1	117.1	117.1	117.1	117.1	117.1
Rotation	half [d]	half [d]	half [d]	half [d]	half [c]	half [c]	half [c]	half [c]
Organ Doses [mGy]								
Bone marrow (red)	0.36	0.31	0.82	0.74	0.36	0.32	0.83	0.74
Colon	0.02	0.07	0.05	0.33	0.03	0.08	0.08	0.29
Lung	2.23	1.67	3.06	2.34	2.48	2.20	3.34	2.99
Stomach	0.46	0.52	2.49	2.39	0.36	0.44	1.74	1.85
Breast	1.92	1.69	2.18	1.93	4.10	3.45	4.53	3.97
Gonads	0.01	0.01	0.02	0.01	0.01	0.01	0.01	0.02
Bladder	0.01	0.01	0.01	0.01	0.01	0.01	0.02	0.02
Oesophagus	1.36	1.03	2.57	1.92	1.26	1.06	2.66	2.15
Liver	0.31	0.23	1.25	0.71	0.63	0.63	2.84	2.48
Thyroid	0.39	0.31	2.84	2.54	0.44	0.38	5.15	4.47
Bone surface	1.27	1.20	2.48	2.36	0.96	0.91	2.06	1.90
Brain	0.02	0.01	0.06	0.04	0.02	0.02	0.06	0.04
Salivary glands	0.08	0.05	0.27	0.17	0.11	0.08	0.32	0.21
Skin	0.36	0.28	0.67	0.55	0.35	0.28	0.66	0.54
Remainder	0.50	0.41	1.21	1.11	0.56	0.49	1.24	1.10
Effective Dose [mSv]	**0.76**	**0.64**	**1.48**	**1.30**	**1.06**	**0.93**	**1.87**	**1.71**

Table 5: Organ and effective doses simulated in the ICRP phantoms for breast CBCT scans and LFOV chest CBCT scans. [c]Half rotation: Gantry angle -180° to +20°. [e]Half rotation: Gantry angle -60° to +140°.

Preset	*Left Breast S10*	*Left Breast S20*	*Right Breast S10*	*Right Breast S20*	*Chest L10*	*Chest L10*	*Chest L20*	*Chest L20*
Isocentre	L breast	L breast	R breast	R breast	Lung centre	Lung centre	Lung centre	Lung centre
Sex M/F	F	F	F	F	F	M	F	M
kV	120	120	120	120	120	120	120	120
Collimator	S10	S20	S10	S20	L10	L10	L20	L20
Filter	F1	F1	F1	F1	F1	F1	F1	F1
Total mAs	117.1	117.1	117.1	117.1	264.0	264.0	264.0	264.0
Rotation	half [e]	half [e]	half [c]	half [c]	full	full	full	full
Organ Doses [mGy]								
Bone marrow (red)	0.32	0.71	0.30	0.69	0.62	0.52	1.26	1.09
Colon	0.02	0.06	0.03	0.08	0.04	0.11	0.10	0.38
Lung	2.04	2.85	2.04	2.66	3.75	3.02	4.82	3.91
Stomach	0.48	2.44	0.36	1.49	0.56	0.64	2.38	2.34
Breast	2.15	2.36	4.28	4.62	3.78	3.14	4.08	3.43
Gonads	0.01	0.02	0.01	0.01	0.01	0.01	0.03	0.02
Bladder	0.01	0.01	0.01	0.02	0.01	0.01	0.03	0.03
Oesophagus	1.20	2.26	1.06	2.22	2.60	2.00	4.68	3.40
Liver	0.37	1.39	0.73	2.85	0.81	0.80	3.14	2.70
Thyroid	0.32	2.41	0.37	4.59	0.67	0.53	6.27	4.87
Bone surface	1.07	2.16	0.70	1.58	1.97	1.87	3.68	3.46
Brain	0.02	0.05	0.02	0.05	0.04	0.03	0.09	0.07
Salivary glands	0.07	0.22	0.09	0.29	0.15	0.11	0.40	0.27
Skin	0.32	0.59	0.29	0.55	0.54	0.44	0.97	0.80
Remainder	0.46	1.12	0.49	1.12	0.84	0.69	1.76	1.56
Left breast	3.18	3.46	3.41	3.74				
Right breast	1.12	1.26	5.14	5.51				
Effective Dose [mSv]	**0.75**	**1.42**	**1.00**	**1.69**	**1.34**	**1.13**	**2.35**	**2.01**

4. Discussion

The simulated organ and effective doses given here correspond to the default protocols provided in the current version of the Elekta XVI CBCT system (XVI version 5.0). Since organ and effective doses scale linearly with mAs, the information given here can be used to calculate doses for other protocols using the same combinations of kV, filter, collimator, rotation angle.

Effective doses for Elekta XVI CBCT that have been previously reported in the literature [6,7,12,13] are for protocols which do not correspond exactly to those simulated here. However comparisons can be made where the protocols differ only in total mAs. For a head and neck scan with the S20 collimator and 36 mAs, Hyer et al [6] and Dufek et al [7] quote effective doses of 0.04 mSv and 0.1 mSv respectively. When scaled appropriately our data give doses of 0.06 mSv and 0.12 mSv for a scans of the male phantom centred on the pituitary and larynx respectively. Scans of the female phantom resulted in doses about 50% higher. For M10 pelvis scans centred on the prostate Hyer et al [6], Dufek et al [7], and Halg et al [12] give effective doses of 2.3 mSv, 4.1 mSv and 3.1 mSv respectively (values normalized to scan with 1040 mAs). The corresponding dose for an M10 pelvis scan from our simulations

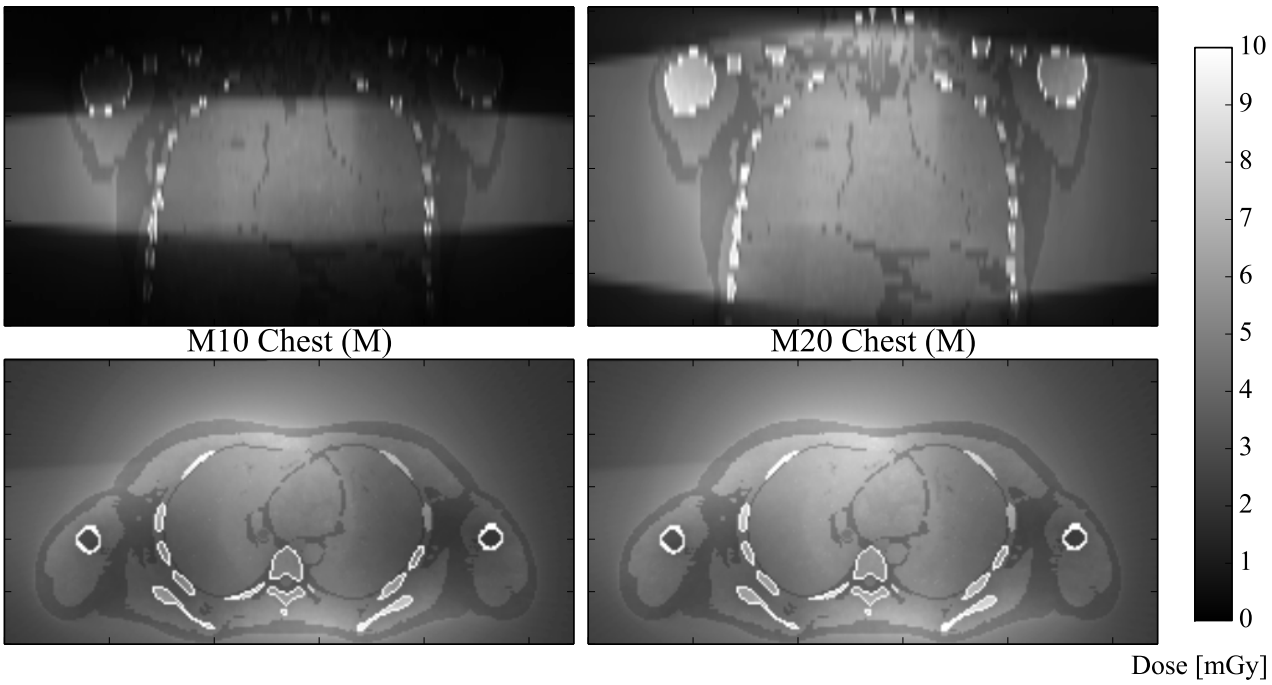

Figure 7. Simulated dose distributions in the ICRP male phantom from MFOV CBCT scans of the chest.

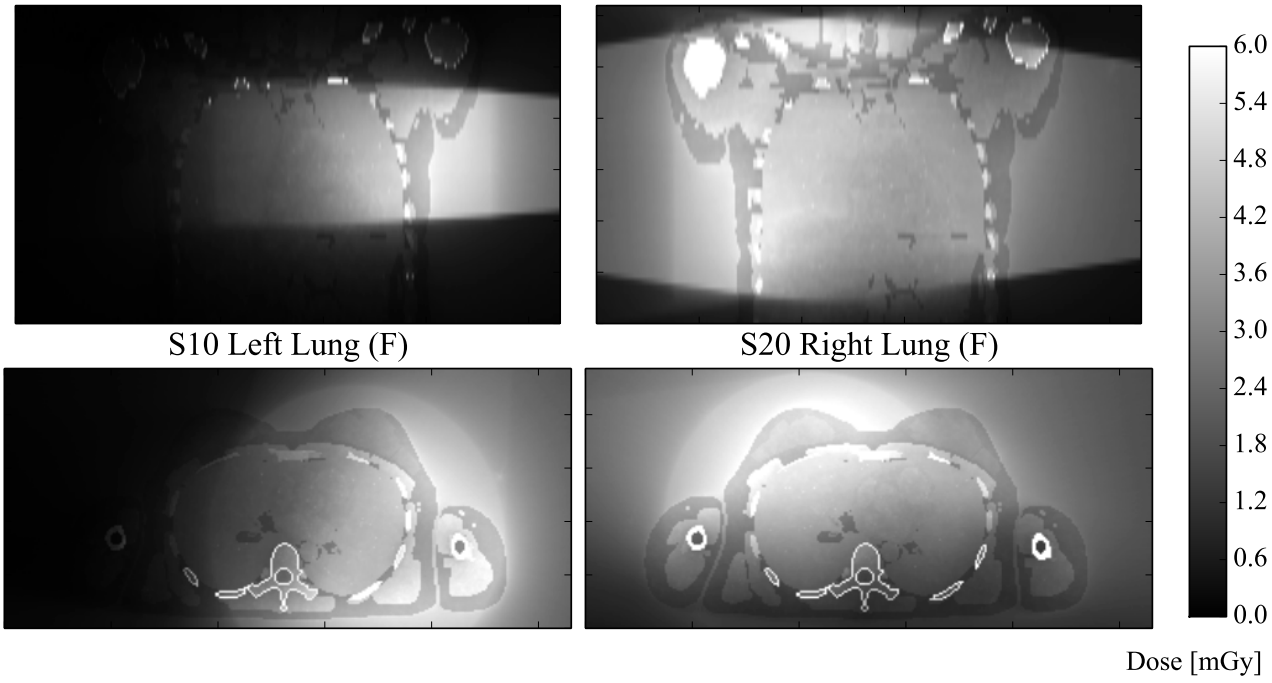

Figure 8. Simulated dose distributions in the ICRP female phantom from SFOV half-rotation CBCT scans of the chest.

is 1.9 mSv. For an M20 chest scan centred on the lungs with 1028 mAs, Hyer et al [6] reports effective dose of 7.15 mSv, which compares to our simulated dose of 10.7 mSv for the male ICRP phantom (increasing to 12.4 mSv for the female phantom). Differences between the doses reported here and those published by other authors may be due to a number of causes, including use of different phantoms, errors due to extrapolating mean organ dose from point dose measurements, and differences in dose output of individual XVI systems.

Many studies of CBCT dose present results for a small number of protocols, typically categorized as head, chest and pelvis [5,6,9,11,13,22]. However a wide variety of protocol variations may be used in clinical practice in both the anatomical location of the scan, and in acquisition parameters such as collimator, filter and partial rotation gantry angles. Table 2 reveals differences in head scan effective dose of approximately a factor of two between those centred on pituitary and larynx. Effective dose for pelvis scans varies markedly between male and female patients and with the FOV length mostly due to the effect on dose to gonads and colon. Patient dose from chest CBCT scans also varies strongly with FOV length, increasing by a factor of two between M10 and M20 scans. Scan position is also important for chest scans, which may be centred on tumour sites in the left or right lung. A few authors [8,21,23,24] have considered the effect on scan dose for off-centre chest scans and for partial rotation chest protocols, although full organ and effective doses have not been presented. Our simulations show how the gantry start and stop angles for partial rotation scans influence the scan dose. For example the rotation used at our institution for imaging of right lung sites (-180° to +20°) results in 25-50 % higher effective dose than the rotation used for imaging left lung sites (-80° to +120°).

We have simulated CBCT scan doses in the male and female ICRP computational phantoms, which are consistent with reference adult anatomical data from ICRP report 89 [37] and are recommended for studies of radiation dose and determination of effective dose. However it should be remembered that the doses presented here are representative for an average patient, and there will be significant variations for individual patients. CT imaging dose is highly dependent on patient size [38] and a number of authors have noted increased CBCT dose for pediatric patients [17,20,39].

CBCT scan doses in this paper are presented as organ and effective doses. It should be acknowledged that use of effective dose to evaluate risk for patients undergoing radiotherapy is non ideal, due to the difficulty of combining with risks from the radiotherapy dose received. However, effective dose is still commonly used to assess IGRT dose burden. The report of AAPM TG-75 [40] recommends effective dose as the only quantity allowing inter-comparison of stochastic risk between different imaging scenarios. Halg et al [12] suggested excluding organs receiving radiotherapy dose greater than 5 Gy from the effective dose calculation to better represent the *additional* risk from imaging. Such a calculation would need to be done on an individual patient basis due to patient specific variations in radiotherapy dose distribution. However, the tables of organ doses presented here would allow re-calculation of effective dose based on a subset of organs as required.

In summary the XVI head and neck presets can be considered low dose with effective doses less than 0.1 mSv. XVI 3D Chest presets have intermediate doses ranging from 1.38

to 3.19 mSv. XVI prostate and pelvis presets have generally higher doses ranging from 2.80 to 7.60 mSv. Four-dimensional (Symmetry) lung scans give the highest imaging dose of 7.88 to 8.30 mSv. The simulated CBCT doses reported here can aid selection of appropriate scanning protocols. For example the clear increase in dose with length of the imaged FOV supports a recommendation to use shorter FOVs whenever possible (e.g. M10 rather than M20 collimator). The expected increase in dose with increased mAs is also observed, for example compare Prostate M15 with Pelvis M15 protocol in table 2. Dose can be minimized by using the M15 Pelvis protocol instead of M15 Prostate. However the trade-off between dose and image quality must be considered [41]; imaging dose should not be reduced below that necessary to produce a clinically acceptable image for the specified purpose.

5. Conclusions

A Monte Carlo model of the Elekta XVI CBCT system has been developed and validated using the Geant4 application for tomographic emission (GATE). The model has been used to simulate patient doses in the ICRP male and female computational phantoms from a comprehensive set of CBCT imaging protocols, including all default protocols in the current version of XVI. Effective doses from head and neck CBCT scans range from 0.03 to 0.09 mSv. Pelvis CBCT scan effective doses range from 2.8 to 7.6 mSv, and medium FOV chest scan doses range from 1.4 to 3.2 mSv. The information presented here will be of use in assessing patient dose from CBCT imaging, as required for justification of imaging procedures. The CBCT MC model developed here may be useful to others for studies of CBCT imaging and dosimetry. Please contact the corresponding author for details of how to obtain the model.

Acknowledgments

This work was supported in part by the UK Medical Research Council (MRC) grant No. MR/L023059/1.

References

[1] Jaffray D A, Siewerdsen J H, Wong J W and Martinez A A 2002 Flat-panel cone-beam computed tomography for image-guided radiation therapy *International Journal of Radiation Oncology*Biology*Physics* **53** (5) 1337–49

[2] McBain C A, Henry A M, Sykes J, Amer A, Marchant T, Moore C M, Davies J, Stratford J, McCarthy C, et al 2006 X-ray volumetric imaging in image-guided radiotherapy: The new standard in on-treatment imaging *International Journal of Radiation Oncology*Biology*Physics* **64** (2) 625–34

[3] Alaei P and Spezi E 2015 Imaging dose from cone beam computed tomography in radiation therapy *Physica Medica* **31** (7) 647–58

[4] Amer A, Marchant T, Sykes J, Czajka J and Moore C 2007 Imaging doses from the Elekta Synergy X-ray cone beam CT system *BJR* **80** (954) 476–82

[5] Song W Y, Kamath S, Ozawa S, Ani S A, Chvetsov A, Bhandare N, Palta J R, Liu C and Li J G 2008 A dose comparison study between XVI and OBI CBCT systems *Medical Physics* **35** (2) 480–6

[6] Hyer D E, Serago C F, Kim S, Li J G and Hintenlang D E 2010 An organ and effective dose study of XVI and OBI cone-beam CT systems *Journal of Applied Clinical Medical Physics* **11** (2)

181–97

[7] Dufek V, Horakova I and Novak L 2011 Organ and effective doses from verification techniques in image-guided radiotherapy *Radiat Prot Dosimetry* **147** (1-2) 277–80

[8] Giaddui T, Cui Y, Galvin J, Yu Y and Xiao Y 2013 Comparative dose evaluations between XVI and OBI cone beam CT systems using Gafchromic XRQA2 film and nanoDot optical stimulated luminescence dosimeters *Medical Physics* **40** (6) 062102

[9] Nobah A, Aldelaijan S, Devic S, Tomic N, Seuntjens J, Al-Shabanah M and Moftah B 2014 Radiochromic film based dosimetry of image-guidance procedures on different radiotherapy modalities *Journal of Applied Clinical Medical Physics* **15** (6) 229–38

[10] ICRP 2007 ICRP publication 103: The 2007 recommendations of the International Commission on Radiological Protection *Annals of the ICRP* **37** (2–4) 1–332

[11] Kan M W K, Leung L H T, Wong W and Lam N 2008 Radiation Dose From Cone Beam Computed Tomography for Image-Guided Radiation Therapy *International Journal of Radiation Oncology*Biology*Physics* **70** (1) 272–9

[12] Halg R A, Besserer J and Schneider U 2012 Systematic measurements of whole-body imaging dose distributions in image-guided radiation therapy *Medical Physics* **39** (12) 7650–61

[13] Moon Y M, Kim H-J, Kwak D W, Kang Y-R, Lee M W, Ro T-I, Kim J K and Jeong D H 2014 Effective dose measurement for cone beam computed tomography using glass dosimeter *Nuclear Engineering and Technology* **46** (2) 255–62

[14] Montanari D, Scolari E, Silvestri C, Graves Y J, Yan H, Cervino L, Roger Rice, Jiang S B and Jia X 2014 Comprehensive evaluations of cone-beam CT dose in image-guided radiation therapy via GPU-based Monte Carlo simulations *Phys. Med. Biol.* **59** (5) 1239

[15] Ding G X, Duggan D M and Coffey C W 2008 Accurate patient dosimetry of kilovoltage cone-beam CT in radiation therapy *Medical Physics* **35** (3) 1135–44

[16] Spezi E, Downes P, Jarvis R, Radu E and Staffurth J 2012 Patient-Specific Three-Dimensional Concomitant Dose From Cone Beam Computed Tomography Exposure in Image-Guided Radiotherapy *International Journal of Radiation Oncology*Biology*Physics* **83** (1) 419–26

[17] Deng J, Chen Z, Roberts K B and Nath R 2012 Kilovoltage Imaging Doses in the Radiotherapy of Pediatric Cancer Patients *International Journal of Radiation Oncology*Biology*Physics* **82** (5) 1680–8

[18] Son K, Cho S, Kim J S, Han Y, Ju S G and Choi D H 2014 Evaluation of radiation dose to organs during kilovoltage cone-beam computed tomography using Monte Carlo simulation *Journal of Applied Clinical Medical Physics* **15** (2) 295–302

[19] Jia X, Yan H, Gu X and Jiang S B 2012 Fast Monte Carlo simulation for patient-specific CT/CBCT imaging dose calculation *Phys. Med. Biol.* **57** (3) 577

[20] Zhang Y, Yan Y, Nath R, Bao S and Deng J 2012 Personalized Assessment of kV Cone Beam Computed Tomography Doses in Image-guided Radiotherapy of Pediatric Cancer Patients *International Journal of Radiation Oncology*Biology*Physics* **83** (5) 1649–54

[21] Winey B, Zygmanski P and Lyatskaya Y 2009 Evaluation of radiation dose delivered by cone beam CT and tomosynthesis employed for setup of external breast irradiation *Medical Physics* **36** (1) 164–73

[22] Palm , Nilsson E and Herrnsdorf L 2010 Absorbed dose and dose rate using the Varian OBI 1.3 and 1.4 CBCT system *Journal of Applied Clinical Medical Physics* **11** (1) 229–40

[23] Alvarado R, Booth J T, Bromley R M and Gustafsson H B 2013 An investigation of image guidance dose for breast radiotherapy *Journal of Applied Clinical Medical Physics* **14** (3) 25–38

[24] Walters B R B, Ding G X, Kramer R and Kawrakow I 2009 Skeletal dosimetry in cone beam computed tomography *Medical Physics* **36** (7) 2915–22

[25] ICRP 2009 ICRP Publication 110: Adult Reference Computational Phantoms *Annals of the*

ICRP **39** (2) 1–166

[26] Martin C J, Abuhaimed A, Sankaralingam M, Metwaly M and Gentle D J 2016 Organ doses can be estimated from the computed tomography (CT) dose index for cone-beam CT on radiotherapy equipment *J. Radiol. Prot.* **36** (2) 215

[27] Morant J, Salvad M, Hernndez-Girn I, Casanovas R, Ortega R and Calzado A 2013 Dosimetry of a cone beam CT device for oral and maxillofacial radiology using Monte Carlo techniques and ICRP adult reference computational phantoms *Dentomaxillofacial Radiology* **42** (3) 92555893

[28] Jan S, Santin G, Strul D, Staelens S, Assi K, Autret D, Avner S, Barbier R, Bardis M, et al 2004 GATE : a simulation toolkit for PET and SPECT *Phys. Med. Biol.* **49** (19) 4543

[29] Sarrut D, Bardis M, Boussion N, Freud N, Jan S, Ltang J-M, Loudos G, Maigne L, Marcatili S, et al 2014 A review of the use and potential of the GATE Monte Carlo simulation code for radiation therapy and dosimetry applications *Medical Physics* **41** (6) 064301

[30] Apostolakis J, Folger G, Grichine V, Howard A, Ivanchenko V, Kosov M, Ribon A, Uzhinsky V and Wright D H 2008 GEANT4 Physics Lists for HEP *IEEE Nuclear Science Symposium Conference Record, 2008. NSS '08* IEEE Nuclear Science Symposium Conference Record, 2008. NSS '08 pp 833–6

[31] Smekens F, Ltang J M, Noblet C, Chiavassa S, Delpon G, Freud N, Rit S and Sarrut D 2014 Split exponential track length estimator for Monte-Carlo simulations of small-animal radiation therapy *Phys. Med. Biol.* **59** (24) 7703

[32] Fedon C, Longo F, Mettivier G and Longo R 2015 GEANT4 for breast dosimetry: parameters optimization study *Phys. Med. Biol.* **60** (16) N311

[33] Boone J M and Seibert J A 1997 An accurate method for computer-generating tungsten anode x-ray spectra from 30 to 140 kV *Medical Physics* **24** (11) 1661–70

[34] Spezi E, Downes P, Radu E and Jarvis R 2009 Monte Carlo simulation of an x-ray volume imaging cone beam CT unit *Medical Physics* **36** (1) 127–36

[35] Williamson J F 1987 Monte Carlo evaluation of kerma at a point for photon transport problems *Medical Physics* **14** (4) 567–76

[36] Downes P, Jarvis R, Radu E, Kawrakow I and Spezi E 2009 Monte Carlo simulation and patient dosimetry for a kilovoltage cone-beam CT unit *Medical Physics* **36** (9) 4156–67

[37] ICRP 2002 ICRP Publication 89: Basic anatomical and physiological data for use in radiological protection: reference values *Ann ICRP* **32** (3-4) 1–277

[38] Boone J M, Strauss, K. J., Cody, D.D., McCollough, C. H., McNitt-Gray, M. F. and Toth, T. L. 2011 *AAPM Report 204: Size-specific dose estimates (SSDE) in pediatric and adult body CT examinations* (AAPM)

[39] Ding G X and Coffey C W 2009 Radiation Dose From Kilovoltage Cone Beam Computed Tomography in an Image-Guided Radiotherapy Procedure *International Journal of Radiation Oncology*Biology*Physics* **73** (2) 610–7

[40] Murphy M J, Balter J, Balter S, Jr J A B, Das I J, Jiang S B, Ma C-M, Olivera G H, Rodebaugh R F, et al 2007 The management of imaging dose during image-guided radiotherapy: Report of the AAPM Task Group 75 *Medical Physics* **34** (10) 4041–63

[41] Yan H, Cervino L, Jia X and Jiang S B 2012 A comprehensive study on the relationship between the image quality and imaging dose in low-dose cone beam CT *Phys. Med. Biol.* **57** (7) 2063